Out-of-Plane Response of Three-span Bridges with Mid-spans Supported by Pins or by Isolators and Excited by Fault-parallel Ground Motion

R.S. Jalali, M. Bahari Jokandan
Dept. of Civil Eng., Faculty of Eng., University of Guilan, P.O. Box 3756, Rasht, Iran

M.D. Trifunac
Dept. of Civil Engineering, Univ. of Southern California, Los Angeles, CA 90089 U.S.A.

SUMMARY:
Out-of-plane response of a symmetric model of a three-span bridge with the mid-span supported by pins or by lead rubber bearings (LRB) excited by fault-parallel ground displacement is considered. The system of nonlinear equations of motion of the model is solved by the fourth-order Runge-Kutta method. For pin-supported mid-span and linear response, with an increasing fundamental period of the bridge, the maximum shear key force decreases, while the maximum drift in piers increases. Depending on the period of the bridge and magnitude of the earthquake, the maximum shear key force may increase by up to 2 times the total weight of the bridge for stiff bridges, and the maximum drift in the piers may increase by 10% for flexible piers. The differential motion effects on maximum shear key force are negligible in the entire range of considered periods ($0.1\ s < T_1 < 1.5\ s$). The wave passage effects lead to increases of about 25% of the maximum drift in piers relative to the drift for synchronous ground motion. For the nonlinear response of piers, depending on the yielding limit of the piers in bending (ϕ_y) and the magnitude of earthquake, for longer fundamental periods of the bridge, the nonlinear behaviour of piers may decrease the maximum shear key force and increase the maximum drift of piers by more than 2 times, compared to the linear system.

Keywords: Out-of-plane response of a three-span bridge, near-fault ground motion, reduction of shear forces in joint keys, isolator deformation, differential strong ground motion.

1. INTRODUCTION

The effects of spatial variations of earthquake motion at multiple supports of structures may be disregarded in many design analyses. However, when the distance between the multiple support points is large (e.g., for bridges, dams, tunnels, long buildings), the effects of differential motions become important and should be considered. Okubo et al. (1983) were among the first to measure and interpret finite ground strains of recorded earthquake motions for plan dimensions representative of intermediate and large buildings. They showed that, for short-period (stiff) structures, finite ground strains lead to increased base shears. Extensions and generalizations of the response-spectrum method have been proposed to account approximately for the wave passage and differential motions along the base of long structures, but these approximations cease to be valid for short-wave excitations. Examples of such extensions are described in several studies involving differential strong motion (Jalali and Trifunac 2009, 2011; Trifunac and Todorovska 1997; Trifunac and Gičev 2006) and strength-reduction factors (Jalali and Trifunac 2007, 2008; Jalali et al. 2007).

Ground motions close to a rupturing fault can be significantly different from those observed further away. In the near-fault zone, ground motions are influenced by the source mechanism and slip direction relative to the site and by the permanent ground displacement resulting from tectonic movement. Research has shown that the impulsive ground motion near an earthquake fault, and specifically the amplitude and period of the velocity pulse, can have a significant effect on the

performance of structures. The purpose of this paper is to investigate the seismic out-of-plane response of a three-span bridge with mid-spans supported by pins or by isolators and excited by fault-parallel ground motion, which results in permanent ground displacement.

2. DYNAMIC MODEL

Shown in Fig. 1a, the model we consider is a symmetric three-span bridge with middle hinges at a and b, consisting of three rigid decks with mass m1, m2, m3, and polar moments of inertia J1, J2, J3, supported by four axially-rigid mass-less piers connected at the top to the deck and at the bottom to the ground by circular rotational and torsional springs (Fig. 1b). The rotational and torsional springs represent the bending and torsional stiffness of the piers. It is assumed that there is no soil structure interaction so that the points on the ground surface, where the piers are supported, move as in the free field of strong motion. At the middle hinges, the rigid decks are connected by rigid shear keys to prevent out-of-plane relative displacement and unseating of the deck, or by lead rubber bearing (LRB) isolators. The mass-less piers are connected to the ground and to the rigid deck by linear circular rotational and torsional dashpots providing the prescribed fraction of critical damping. Rotation of the piers is assumed to be small enough that the interaction between in-plane (longitudinal) and out-of-plane (transverse) motions of the rigid deck can be disregarded. The bridge is acted upon by the acceleration of gravity, g, and is excited by differential out-of-plane and torsional ground motions. We define the parameters of the model as follows:

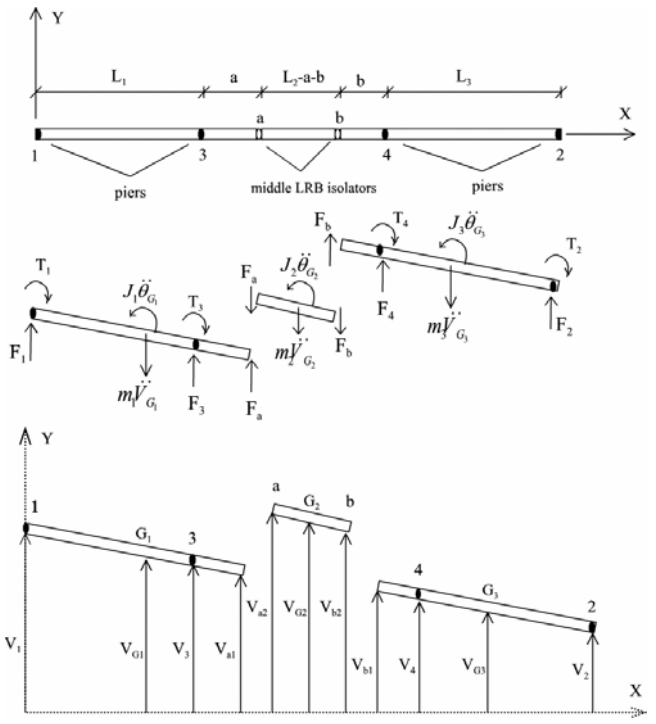

Fig. 1a Plan view of the bridge with the mid-span supported by LRB isolators.

k_ϕ = Initial bending stiffness of the piers;

c_ϕ = Linear bending damping coefficient of the piers;

k_{T_c} = Initial torsional stiffness of the piers;

c_{T_c} = Linear torsional damping coefficient of the piers;

m_i = Mass of $i-th$ rigid deck;

$m = m_1 + m_2 + m_3$ = Total mass of the bridge;

$L_1 = L_2 = L_3 = L$ = Length of each span,

$a = b = L/5$ = distance between middle hinge and the nearest pier;

J_i = Polar moment of inertia of $i-th$ rigid deck;

h = The height of bridge;

ϕ_i = Rotational angle of $i-th$ pier;

v_{g_i}, θ_{g_i} = The free field out-of-plane and torsional motions of the ground surface at the base of $i-th$ pier $(i = 1,2,3,4)$;

V_{G_i}, θ_{G_i} = Absolute out-of-plane and torsional motions of the centre of gravity of $i-th$ rigid deck $(i = 1,2,3)$;

F_a, F_b = Force in shear key or LRB isolator at hinges a and b, respectively;

Δ_a, Δ_b = Relative out-of-plane displacement or shear deformation of LRB isolators at hinges a and b, respectively.

Based on Fig.1b, for the bridge with the mid-span supported by LRB isolators, the absolute out-of-plane displacements and torsion of the centre of gravity of three rigid decks are,

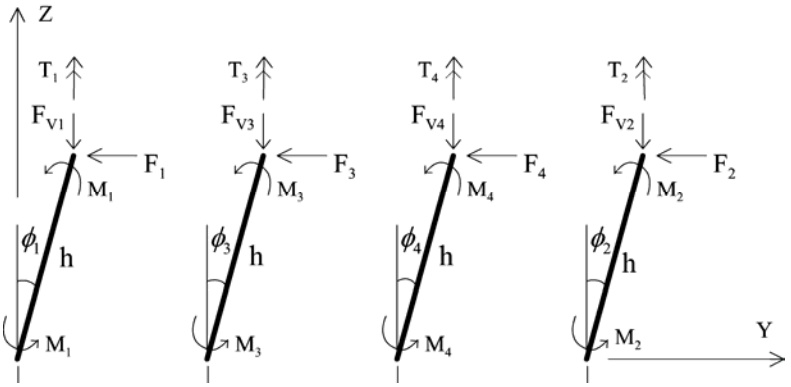

Fig. 1b Side view of the bridge piers.

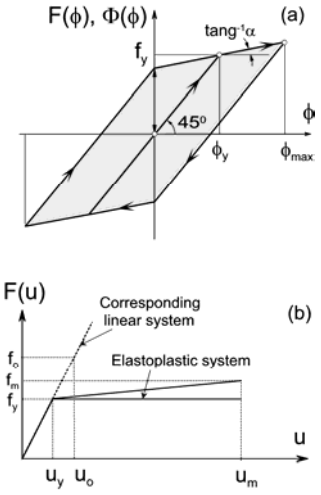

Fig. 2 Bilinear rotational stiffness of the elasto- plastic system.

$$
\begin{aligned}
&V_{G_1}=\frac{(L-a)}{2L}V_1+\frac{(L+a)}{2L}V_3=\frac{(L-a)}{2L}(V_{g_1}+h\sin\phi_1)+\frac{(L+a)}{2L}(V_{g_3}+h\sin\phi_3)\\
&V_{G_3}=\frac{(L-b)}{2L}V_2+\frac{(L+b)}{2L}V_4=\frac{(L-b)}{2L}(V_{g_2}+h\sin\phi_2)+\frac{(L+b)}{2L}(V_{g_4}+h\sin\phi_4)\\
&\Delta_a=V_{a_2}-V_{a_1}\Rightarrow V_{a_2}=V_{a_1}+\Delta_a=\frac{-a}{L}(V_{g_1}+h\sin\phi_1)+\frac{L+a}{L}(V_{g_3}+h\sin\phi_3)+\Delta_a\\
&\Delta_b=V_{b_2}-V_{b_1}\rightarrow V_{b_2}=V_{b_1}+\Delta_b=\frac{-b}{L}(V_{g_2}+h\sin\phi_2)+\frac{L+b}{L}(V_{g_4}+h\sin\phi_4)+\Delta_b\\
&V_{G_2}=\frac{V_{a_2}+V_{b_2}}{2}=\frac{-a}{2L}(V_{g_1}+h\sin\phi_1)+\frac{L+a}{2L}(V_{g_3}+h\sin\phi_3)-\frac{b}{2L}(V_{g_2}+h\sin\phi_2)\\
&+\frac{L+b}{2L}(V_{g_4}+h\sin\phi_4)+\frac{\Delta_a+\Delta_b}{2}\\
&\theta_{G_1}=\sin^{-1}(\frac{V_1-V_3}{L})=\sin^{-1}\left\{\frac{1}{L}\left[(V_{g_1}-V_{g_3})+h(\sin\phi_1-\sin\phi_3)\right]\right\}\\
&\theta_{G_2}=\sin^{-1}(\frac{V_{a_2}-V_{b_2}}{L-a-b})=\sin^{-1}\{\frac{1}{(L-a-b)}[\frac{-a}{L}(V_{g_1}+h\sin\phi_1)+\frac{(L+a)}{L}(V_{g_3}+h\sin\phi_3)\\
&+\frac{b}{L}(V_{g_2}+h\sin\phi_2)-\frac{(L+b)}{L}(V_{g_4}+h\sin\phi_4)+\Delta_a-\Delta_b]\}\\
&\theta_{G_3}=\sin^{-1}(\frac{V_4-V_2}{L})=\sin^{-1}\left\{\frac{1}{L}\left[(V_{g_4}-V_{g_2})+h(\sin\phi_4-\sin\phi_2)\right]\right\}
\end{aligned}
\quad . \quad (1)
$$

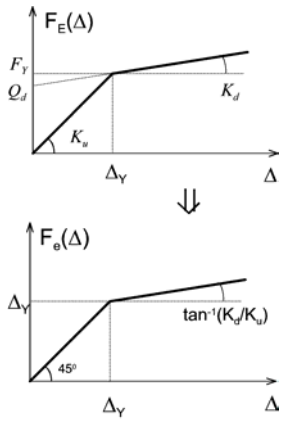

Fig. 3 Force-displacement relationship for LRB isolators.

The equilibrium equations of three rigid decks are

$$
\sum F=0\Rightarrow\begin{cases}F_1+F_3+F_a-m_1\ddot{V}_{G_1}=0\\ F_a+F_b+m_2\ddot{V}_{G_2}=0\\ F_2+F_4+F_b-m_3\ddot{V}_{G_3}=0\end{cases}. \quad (2)
$$

$$
\sum M_G=0\Rightarrow\begin{cases}T_1+T_3+F_1(\frac{L+a}{2})\cos\theta_{G_1}-J_1\ddot{\theta}_{G_1}\\ -F_3(\frac{L-a}{2})\cos\theta_{G_1}-F_a(\frac{L+a}{2})\cos\theta_{G_1}=0\\ (F_b-F_a)\frac{(L-a-b)}{2}\cos\theta_{G_2}-J_2\ddot{\theta}_{G_2}=0\\ T_2+T_4+F_b\frac{(L+b)}{2}\cos\theta_{G_3}+F_4\frac{(L-b)}{2}\cos\theta_{G_3}\\ -F_2\frac{(L+b)}{2}\cos\theta_{G_3}-J_3\ddot{\theta}_{G_3}=0\end{cases}, \quad (3)
$$

where F_a and F_b are shear forces in LRB isolators at hinges defined as follows,

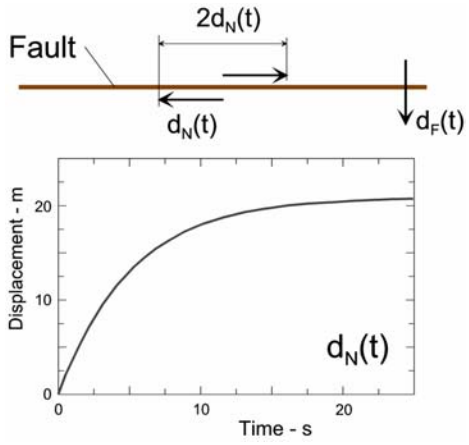

Fig. 4 Fault-parallel displacement for M = 7.

$$F_a = F_E(\Delta_a) + C_u\dot{\Delta}_a = K_u F_e(\Delta_a) + C_u\dot{\Delta}_a$$
$$F_b = F_E(\Delta_b) + C_u\dot{\Delta}_b = K_u F_e(\Delta_b) + C_u\dot{\Delta}_b \quad . \qquad (4)$$

K_u and C_u are elastic stiffness and viscous damping of LRB isolators respectively. $F_E(\Delta)$, and $F_e(\Delta)$ are nonlinear functions of the type described in Fig. 3. K_d is the post-yield stiffness; Q_d is the zero-displacement force-intercept; F_Y is the yield force; Δ_Y is the yield displacement of the isolator. The yield strength of the isolator is associated with the characteristic strength by the relation $F_Y = Q_d/(1-K_d/K_u)$. K_d of the isolator is designed in such a way as to provide the specific value of

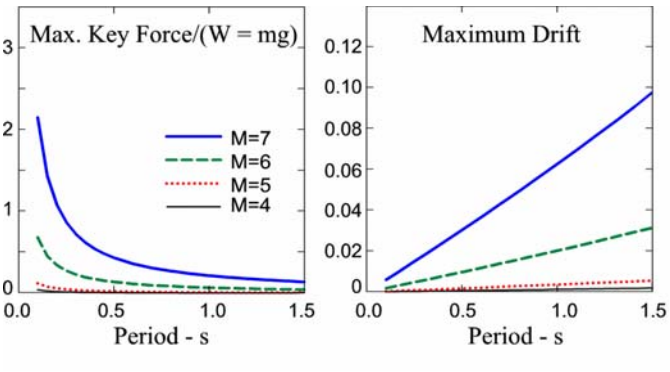

Fig. 5 Maximum linear shear key force (left) and drift of piers (right), versus system period, for zero time lag ($\tau = 0$) and fault-parallel displacement during earthquakes with M = 4 to 7.

the isolation period, T_E expressed as $T_E = 2\pi\sqrt{\frac{W}{K_d g}}$, where W is the weight acting on an individual isolator; and g is the gravitational acceleration constant. The viscous damping of the isolator, C_u is evaluated by the damping ratio, ξ_E expressed as $\xi_E = C_u/(2M\omega_E)$, where M is the mass acting on an individual isolator and $\omega_E = 2\pi/T_E$ is the base isolation frequency. There have been several studies investigating the optimum design values for the lead rubber bearings (Park and Otsuka 1999; Naeim and Kelly 1999; Jangid 2006). Hameed et al. (2008) recommended $Q_d/W = 0.05$ to 0.10, $T_d = 2.5$ to 3.0 sec, and $K_u/K_d = 8$ to 10 for the severe earthquakes having intense long duration pulses with low frequency contents and records with low PGA/PGV ratios (<7.5 s-1). In this paper we have assumed the following values for the LRB isolators $Q_d/W = (0.05+0.1)/2 = 0.075$, $T_E = (2.5+3.0)/2 = 2.75$, $K_u/K_d = (8+10)/2 = 9$, and $\xi_E = 0.05$.

The equilibrium equation of $i-th$ pier is

$$\sum M = 0 \Rightarrow 2M_i + F_i h\cos\phi_i - F_{V_i} h\sin\phi_i = 0 \Rightarrow F_i = F_{V_i}\tan\phi_i - \frac{2M_i}{h\cos\phi_i} \quad . \qquad (5)$$

By assuming uniform distribution of mass over the length of the bridge decks we can approximately determine F_{V_i} as follows,

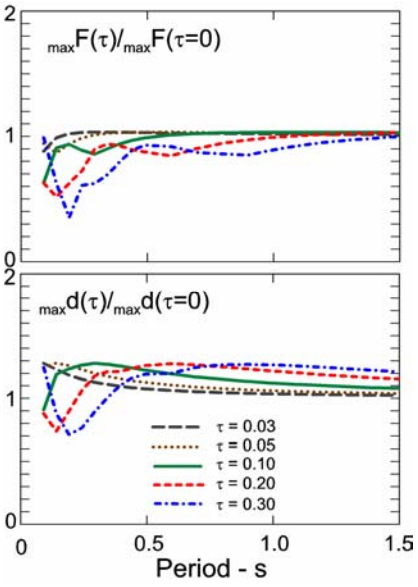

Fig. 6 Magnification factor for maximum linear shear force (top), and drift of piers (bottom) for a bridge with middle shear keys, excited by ground motion with different time lags (0.03 to 0.3 s)

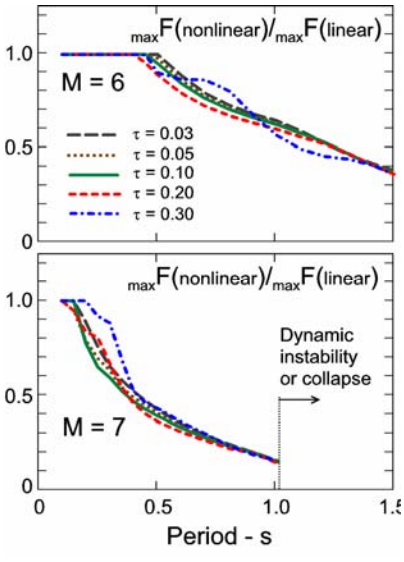

Fig. 7 Ratios of maximum nonlinear to linear shear forces in middle shear keys for ϕ_y=0.01, magnitudes M = 6 and 7 and time lags 0.03 to 0.3 s.

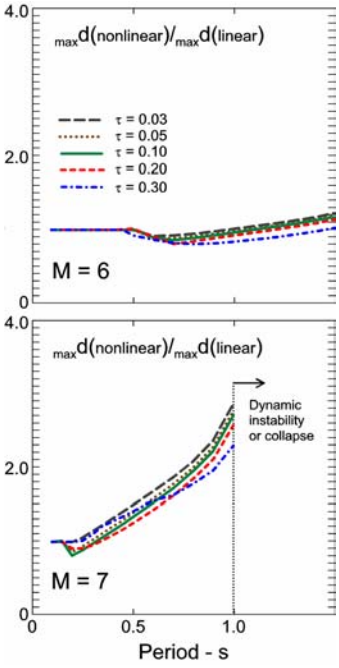

Fig. 8 Ratios of maximum nonlinear to linear drifts of bridge piers for ϕ_y=0.01.

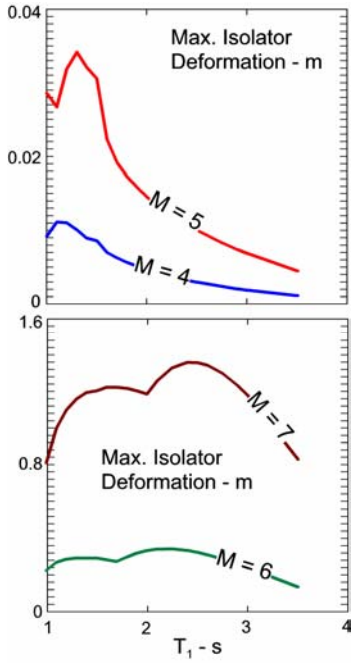

Fig. 9 Maximum isolator deformations (MID) for M = 4 to 7 and zero time lags.

$$
\begin{aligned}
F_{V_1} &= [\frac{m_1}{2} - (m_1 + m_2)\frac{a}{2L}]g \\
F_{V_2} &= [\frac{m_3}{2} - (m_2 + m_3)\frac{b}{2L}]g \\
F_{V_3} &= (m_1 + m_2)(\frac{L+a}{2L})g \\
F_{V_4} &= (m_2 + m_3)(\frac{L+b}{2L})g
\end{aligned}
\quad . \qquad (6)
$$

The bending and torsional moments of piers are

$$
\begin{aligned}
M_i &= K_\phi F(\phi_i) + C_\phi \dot{\phi}_i \\
T_1 &= K_{T_C}\Phi(\theta_{g_1} - \theta_{G_1}) + C_{T_C}(\dot{\theta}_{g_1} - \dot{\theta}_{G_1}) \\
T_2 &= K_{T_C}\Phi(\theta_{g_2} - \theta_{G_3}) + C_{T_C}(\dot{\theta}_{g_2} - \dot{\theta}_{G_3}) \\
T_3 &= K_{T_C}\Phi(\theta_{g_3} - \theta_{G_1}) + C_{T_C}(\dot{\theta}_{g_3} - \dot{\theta}_{G_1}) \\
T_4 &= K_{T_C}\Phi(\theta_{g_4} - \theta_{G_3}) + C_{T_C}(\dot{\theta}_{g_4} - \dot{\theta}_{G_3})
\end{aligned}
\quad , \qquad (7)
$$

where $F(\phi)$, and $\Phi(\phi)$ are nonlinear function of the type described in Fig. 2. From (1), (4), (5), (6), and (7) and by considering

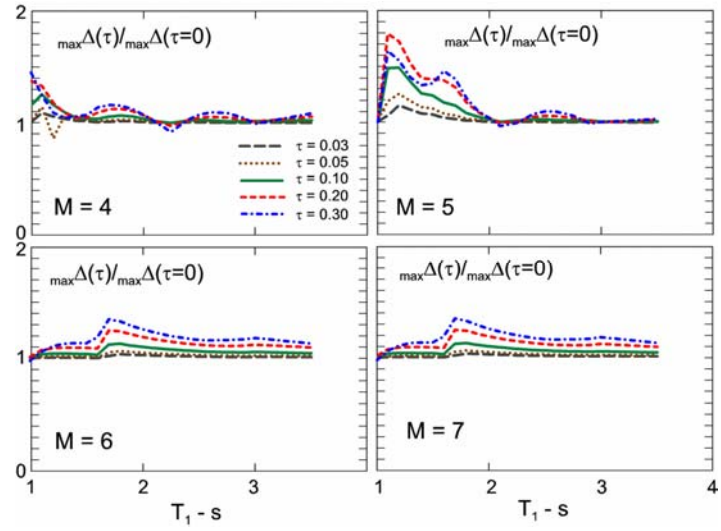

Fig. 10 Magnification factors of maximum isolator deformation (MID) caused by non-zero lag times (0.03 to 0.3 s), and for excitations by fault-parallel displacement corresponding to earthquakes with M = 4 to 7.

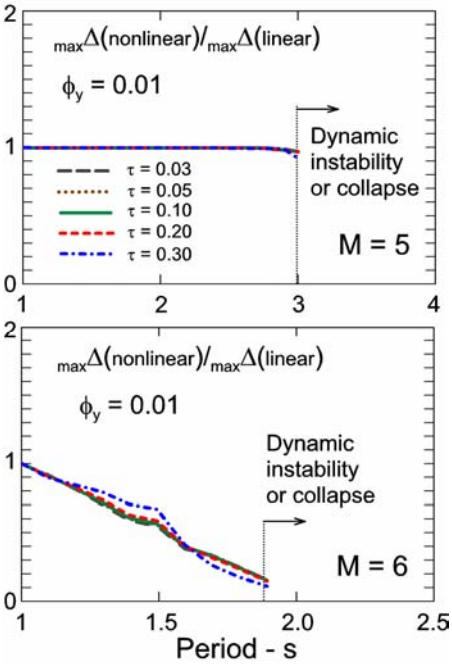

Fig. 11 Ratios of maximum nonlinear to linear isolator deformations for different time lags and, ϕ_y = 0.01. and M = 5 and 6.

$$m = m_1 + m_2 + m_3$$
$$\alpha_{m_i} = \frac{m_i}{m} \qquad (8)$$

we can write the equilibrium equations of the bridge for $\phi_1, \phi_2, \phi_3, \phi_4, \Delta_a$ and Δ_b as follows:

$$\begin{bmatrix} c_{11} & c_{12} & c_{13} & c_{14} & c_{15} & c_{16} \\ c_{21} & c_{22} & c_{23} & c_{24} & c_{25} & c_{26} \\ c_{31} & c_{32} & c_{33} & c_{34} & c_{35} & c_{36} \\ c_{41} & c_{42} & c_{43} & c_{44} & c_{45} & c_{46} \\ c_{51} & c_{52} & c_{53} & c_{54} & c_{55} & c_{56} \\ c_{61} & c_{62} & c_{63} & c_{64} & c_{65} & c_{66} \end{bmatrix} \begin{Bmatrix} \ddot{\phi}_1 \\ \ddot{\phi}_2 \\ \ddot{\phi}_3 \\ \ddot{\phi}_4 \\ \ddot{\Delta}_a \\ \ddot{\Delta}_b \end{Bmatrix} + \begin{Bmatrix} c_{17} \\ c_{27} \\ c_{37} \\ c_{47} \\ c_{57} \\ c_{67} \end{Bmatrix} = \begin{Bmatrix} 0 \\ 0 \\ 0 \\ 0 \\ 0 \\ 0 \end{Bmatrix}, \quad (9)$$

where c_{ij} is a nonlinear function of $\phi_i, \Delta_a, \Delta_b$, and input ground motion.

If we suppose that the stiffness of the LRB isolator is infinite, then it acts like a pin $(\Delta_a = \Delta_b = 0)$, and the system approaches the behaviour of a bridge with the mid-span supported by rigid shear keys. In this condition the equilibrium equations of the system (Eq. 9) would change to the following equation (10),

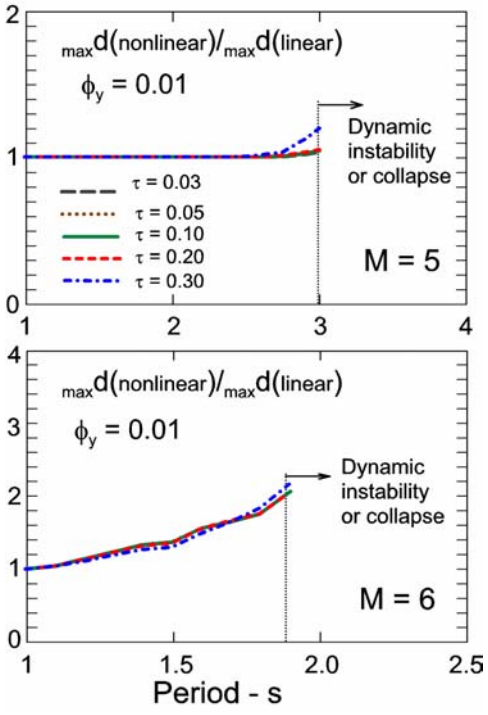

Fig. 12 Ratios of maximum nonlinear to linear drifts in piers of the bridge with middle isolators for strong motion with M = 5 and 6 and for ϕ_y = 0.01.

$$\begin{bmatrix} c_{11} & c_{12} & c_{13} & c_{14} \\ c_{21} & c_{22} & c_{23} & c_{24} \\ c_{31} & c_{32} & c_{33} & c_{34} \\ c_{41} & c_{42} & c_{43} & c_{44} \end{bmatrix} \begin{Bmatrix} \ddot{\phi}_1 \\ \ddot{\phi}_2 \\ \ddot{\phi}_3 \\ \ddot{\phi}_4 \end{Bmatrix} + \begin{Bmatrix} c_{15} \\ c_{25} \\ c_{35} \\ c_{45} \end{Bmatrix} = \begin{Bmatrix} 0 \\ 0 \\ 0 \\ 0 \end{Bmatrix}. \qquad (10)$$

where c_{ij} is nonlinear function of ϕ_i, and input ground motion. The system of nonlinear equations of motion of the model in Fig. 1, which is described by equations (9), and (10), can be solved by numerical methods. We chose the fourth-order Runge-Kutta method because of its self-starting feature and the long-range stability. In this method, the time domain is divided into n equally spaced intervals, where n is chosen based on the requirement to have at least 20 points per period of excitation or per fundamental period of the structure, whichever is smaller. Each of these equally spaced intervals is further subdivided into 2^r intervals, where r varies from 1 to 9, to reach the desired accuracy. The parameter r is chosen so that the relative error between the solutions for the neighbouring two values of n is less than 1%, and then the larger n of the two is adopted for the calculations.

3. NEAR-FAULT GROUND MOTION

We describe the ground motion by d_N (fault-parallel permanent displacement) and select the amplitudes and duration consistent with the variables, which describe near fault motions (Haskell 1969). Fig. 4 shows a fault schematically, with the displacement, d_N, describing monotonic growth of the displacement toward the permanent static offset. Further discussion and motivation for selecting this simple strong motion displacement functions is described in our previous work (Jalali and Trifunac 2007, 2008, 2009). An important physical characteristic of d_N is the large initial velocity associated with onset of these motions. It is proportional to the stress drop on the fault and even in the presence of nonlinear site response it can be hundreds of cm/s (Trifunac 1993, 1998, 2009). We describe this fault-parallel permanent displacement as follows,

$$d_N(t) = \frac{A_N}{2}(1 - e^{-\frac{t}{\tau_N}}) \qquad (11)$$

where the values of A_N, and τ_N, versus earthquake magnitudes, are given in Trifunac (1993). The amplitude of d_N has been studied in numerous regression analyses in terms of the observed surface expressions of fault slip. It is traditionally presented as average dislocation amplitudes, $\bar{u}$, and is related to d_N, as $\bar{u} = 2d_N$ (see top part of Fig. 4).

4. STRUCTURAL RESPONSE

The nature of relative motion of individual column foundations or of the entire foundation system will depend on the type of foundation and stiffness of the connecting beams and slabs, the characteristics

of the soil surrounding the foundation, the type of incident waves, and the direction of wave arrival (Trifunac 1997; Trifunac and Todorovska 1997). In reality, at the base of each column, the motion has six degrees of freedom, which will depend on the foundation-soil interaction and on the degree to which the nonlinear deformations occur in the structure and in the soil. In this research, we consider simultaneous action of out-of-plane (in Y-axis) and torsional (around Z-axis) components of near-fault ground motion at the base (v_{g_i}, θ_{g_i}) with magnitudes M = 4 to 7, but we disregard the effects of foundation-soil interaction. We assume that the structure is near the fault and that the longitudinal axis of the structure (X-axis) coincides with the radial direction (r-axis) of the propagation of waves from the earthquake source so that the absolute displacements of the bases of columns are different, because of the wave passage. However, we assume that the ground motion can be described approximately by linear wave motion. By considering the wave propagation from left to right in Fig.1a, we assume that the excitations at all piers have the same amplitude but differ in terms of phase. The phase difference (or time delay) between the four ground motions depends on the distance between piers and the horizontal phase velocity of the incident waves. As is seen from Fig.1a, the system is excited by differential out-of-plane and torsional ground motions, $v_{g_i}, \theta_{g_i}, i = 1, 4$, at the four bases, so that,

$$
\begin{aligned}
v_{g_2}(t) &= v_{g_1}(t-\tau) \\
v_{g_3}(t) &= v_{g_1}(t-\tau/3) \\
v_{g_4}(t) &= v_{g_1}(t-2\tau/3) \\
\theta_{g_2}(t) &= \theta_{g_1}(t-\tau) \quad , \qquad (12) \\
\theta_{g_3}(t) &= \theta_{g_1}(t-\tau/3) \\
\theta_{g_4}(t) &= \theta_{g_1}(t-2\tau/3) \\
\tau &= (3L)/C_x
\end{aligned}
$$

where C_x is the horizontal phase velocity of incident waves. The functional form of $v_{g_i}(t)$ is defined by Eq. (11) for the fault-parallel displacement. The torsional component of the ground motion is approximated by (Lee and Trifunac 1985)

$$\theta_g(t) = (-\frac{1}{C_x})\dot{v}_g(t)\,, \qquad (13)$$

where $\dot{v}_g(t)$ is the out-of-plane velocity of ground motion. For body waves, C_x will depend on the shear wave velocity in the half space (β) and the incident angle (γ). For surface waves, C_x will depend on the dispersion characteristics of the medium ($C_x(\omega)$ will be different for each of the surface wave modes). For plane waves, the value of C_x varies between β and infinity ($\beta < C_x < \infty$). In this research, the horizontal phase velocity will be assumed to vary between 300 m/s and infinity ($300 < C_x < \infty$). For illustrations in this work, it is assumed that L_1=L_2=L_3=L=30 m, and for different phase velocities different time delays are selected ($\tau =$ 0.03 to 0.30 s). The height of the bridge is h = 6 m. The torsional stiffness and damping of the piers are assumed to be zero ($K_{TC} = C_{TC} = 0$). It should be mentioned that the contributions of all modes of the bridge are included in all analyses and the damping ratio of the first mode is supposed to be $\zeta_1 = 0.02$. The period of the first mode of the bridge with the mid-span supported by pins or rigid shear keys varies between T_1=0.1 and 1.5 s. The main period of the bridge with the mid-span supported by LRB isolators varies between T_1=1.0 and 3.5 s. The response of the bridge is illustrated with respect to T_1. In nonlinear analyses, the material behaviour of piers in bending is assumed to be elasto-plastic and the yielding limit of rotational springs of piers is supposed to be $\phi_y = 0.01$.

5. RESULTS AND CONCLUSIONS

Based on the equations (9) and (10), we analysed the response of a three-span bridge with the mid-span supported by isolators or by shear keys, respectively. The response of the bridge with middle shear keys is shown in Figs. 5 through 8, and the response of the bridge with middle isolators is shown in Figs. 9 through 12.

For bridge with the mid-span supported by shear keys, under synchronous fault-parallel ground motion, it is seen from Fig. 5 that by increasing of the system period, the maximum linear shear key force decreases while the maximum linear drift of piers increases. In this condition, the maximum linear shear key force and drift in piers may increase by up to 2 times the total weight of the bridge and by 10% for stiff ($T_1 = 0.1$ s) and soft ($T_1 = 1.5$ s) bridges, respectively. In Fig. 6 we show the wave passage effects on the maximum linear shear key force and drift in piers of bridges excited by fault-parallel motion during magnitude M=7 earthquake. For this purpose we have defined the magnification factor $\left[MF = \max response(\tau \neq 0) / \max reponse(\tau = 0)\right]$ as the ratio of maximum response of the bridge for differential ground motion to the corresponding value of the system response to synchronous ground motion. As it is seen from Fig. 6 (top) for fault-parallel ground motion the differential motion effect on maximum linear shear key force of bridge is negligible in the entire range of considered periods. It is seen from Fig. 6 (bottom) that the wave passage of translational out-of-plane excitation by fault-parallel ground motion tends to increase the drift in the piers of the bridge by about 25% and, depending on the time delay and the combined action of out-of-plane and torsional responses, this amplification can occur in the entire range of considered periods ($0.1 < T_1 < 1.5$).

By assuming the material nonlinearity associated with bending of piers we show the ratios of nonlinear to linear responses of the bridge in Figs. 7 and 8. It is seen that depending on the system period of the bridge, yielding limit of the piers in bending ϕ_y, and earthquake magnitude, the amplitude of the responses become sensitive to action of the gravity load. For large magnitudes the destabilizing effect of gravity and of horizontal excitation lead to conditions that are close to collapse. It is seen from Figs. 7 and 8 that, for fault-parallel ground motion, the nonlinear behaviour of piers tends to decrease the maximum shear key forces and to increase in maximum drifts of the piers of the bridge by more than 2 times with respect to the equivalent linear system.

For a bridge with the mid-span supported by isolators, under synchronous fault-parallel ground motion, it is seen from Fig. 9 that with an increasing system period, the isolator deformation decreases for small earthquakes, but tends more toward constant levels for larger motions. Depending on the system period of the bridge and magnitude of earthquake, the maximum drift in piers may increase by up to 25% in the range of considered periods ($1.0 < T_1 < 3.5$). Depending on the magnitude of earthquake, the maximum isolator deformation is achieved at different periods. For small magnitudes, the maximum isolator deformation is between 1.1 cm and 3.5 cm for M = 4, and 5 respectively, and takes place for periods $T_1 = 1.1–1.3$ s. For large magnitudes, the maximum isolator deformation is 35 cm to 1.35 m for M = 6 and 7 respectively, and takes place for period $T_1 = 2–2.5$ s. The maximum deformation is important for proper design of LRB isolators and of the width of the pier to prevent unseating of the decks. Large transverse displacement is expected near active faults. As Jonsson et al. (2010) have shown for the earthquake of 29 May 2008 in Iceland, the Oseyrar Bridge was hit and damaged by near-fault ground motion because of small gaps between the stoppers and the superstructure. The calculated peak shear force in the concrete stoppers of the bridge was about 1.5–3.5 times the total weight of the bridge and led to cracking and smashing of the concrete blocks at the top of the piers.

It is seen from Fig. 10 that the wave passage effect on the maximum isolator deformation is more noticeable for small earthquakes (M = 4 and 5) than for large earthquakes (M = 6 and 7). For small earthquakes the wave passage effect can amplify the maximum isolator deformation of a bridge by 1.5–1.8 times for periods $T_1 < 1.5–2.0$ s, while for large earthquakes, this amplification can reach 1.3 and takes place for periods $T_1 > 1.5–2.0$ s. It is seen from Figs. 11 and 12 that the nonlinear behaviour

of piers tends to decrease the maximum isolator deformation and to increase the maximum drifts of piers by more than 2 times, relative to the linear system.

REFERENCES

Hameed, A., Koo, M.S., Dai Do, T. and Jeong, J.H., (2008), Effect of Lead Rubber Bearing Characteristics on the Response of Seismic-isolated Bridges, *KSCE Journal of Civil Engineering,* 12(3), 187-196.

Haskell, N.A. (1969). Elastic displacements in the near field of a propagating fault, *Bull. Seismol. Soc. Amer.,* 59(2), 956-980.

Jalali, R. S., and M. D. Trifunac (2007). Strength-reduction factors for structures subjected to differential near-source ground motion, *Indian Society of Earthquake Technology Journal*, 44(1), 285–304.

Jalali, R. S., and M. D. Trifunac (2008). A note on strength reduction factors for design of structures near earthquake faults, *Soil Dyn. and Earthquake Eng*., 28(3), 212–222.

Jalali, R. S., and M. D. Trifunac (2009). Response Spectra for Near-source, Differential and Rotational Strong Ground Motion, *Bull. Seism. Soc. Amer*., 99(2B), 1404-1415.

Jalali, R. S., and M. D. Trifunac (2011). A note on the wave-passage effects in out-of-plane response of long structures to strong earthquake pulses, Soil Dyn. and Earthquake Eng., 31(12), 640-647.

Jalali, R. S., M. D. Trifunac, G. Ghodrati Amiri, and M. Zahedi (2007).Wave-passage effects on strength-reduction factors for design of structures near earthquake faults, *Soil Dynamics and Earthquake Engineering,* 27(8), 703–711.

Jangid, R.S., (2006). Optimum lead-rubber bearings for near-fault motions, *Engineering Structures*, 29(10), 2503-2513.

Jonsson, M.H., Bessason, B., and Haflidason, E. (2010). Earthquake response of a base-isolated bridge subjected to strong near-fault ground motion, *Soil Dynamics and Earthquake Engineering*, 30, 447-455.

Lee, V. W. and M. D. Trifunac (1985). Torsional accelerograms, *Soil Dyn. Earthq. Eng*., 4(3), 132-9.

Naeim, F. and Kelly, J. M., (1999). *Design of Seismic Isolated Structures: From Theory to Practice*, Wiley, Chichester, England.

Okubo, T., Arakawa, T., and Kawashima, T. (1983). Preliminary analysis of finite ground strains induced during earthquake and effect of spatial ground motions on structural response, *Int. Symp. on Lifeline Earthquake Eng., 4th U.S. Natl. Conf. on Pressure Vessels and Piping Tech.,* ASME, Portland, Oregon.

Park, J. and Otsuka, H., (1999). Optimal yield level of bilinear seismic isolation devices, *Earthquake Engineering and Structural Dynamics,* 28, 941-955.

Trifunac, M. D. (1993). Broad band extension of Fourier amplitude spectra of strong motion acceleration, *Dept. of Civil Eng. Report CE 93-01*, (http://www.usc.edu/dept/civil_eng/Earthquake_eng/), Univ. of Southern California, Los Angeles, California.

Trifunac, M. D. (1997). Relative earthquake motion of building foundations, *Journal of Structural Eng. ASCE* 123(4), 414–422.

Trifunac, M. D. (1998). Stresses and intermediate frequencies of strong motion acceleration, *Geofizika*, 14, 1–27.

Trifunac, M. D. (2009). The role of strong motion rotations in the response of structures near earthquake faults, *Soil Dynamics and Earthquake Eng.,* 29(2), 382–393.

Trifunac, M. D., and V. Gičev (2006). Response spectra for differential motion of columns, Paper II: Out-of-plane response, *Soil Dynamics and Earthquake Engineering*, 26(12), 1149–1160.

Trifunac, M. D., and M. I. Todorovska (1997). Response spectra and differential motion of columns, *Earthquake Eng. and Structural Dyn.,* 26(2), 251–268.